

## Supporting Information

### **A sensitive electrochemical aptasensor based on the co-catalysis of hemin/G-quadruplex, platinum nanoparticles and flower-like MnO<sub>2</sub> nanospheres functionalized multi-walled carbon nanotubes**

**Wenju Xu\*, Shuyan Xue, Huayu Yi, Pei Jing, Yaqin Chai, Ruo Yuan\***

*Key Laboratory of Luminescent and Real-Time Analytical Chemistry (Southwest University), Ministry of Education, School of Chemistry and Chemical Engineering, Southwest University, Chongqing 400715, PR China*

#### **EXPERIMENTAL SECTION**

##### **Reagents and materials**

Thrombin (TB), hemin, toluidine blue (Tb), gold chloride (HAuCl<sub>4</sub>), chloroplatinic acid (H<sub>2</sub>PtCl<sub>6</sub>), bovine serum albumin (BSA, 96-99%), hemoglobin (Hb), human IgG, N-(3-dimethylaminopropyl)-N'-ethylcarbodiimidehydrochloride (EDC) and N-hydroxy succinimide (NHS) were all purchased from Sigma-Aldrich Chemical Co. (St. Louis, MO, USA). 3-aminopropyltriethoxysilane (APTES, 98%) were obtained from Beijing Bailingwei Chemical Technology Co., Ltd. (Beijing, China). Potassium permanganate (KMnO<sub>4</sub>) was purchased from Chengdu Kelong Chemical Reagent Company (Chengdu, China). Glutaraldehyde (GA) and oleic acid was obtained from Beijing Chemical Reagent Co. (Beijing, China). Multi-walled carbon nanotubes

(MWCNTs) (>95% purity) were obtained from Chengdu Organic Chemicals Co., Ltd., of the Chinese Academy of Science (Chengdu, China). The human serum samples were from the Xinqiao Hospital (Chongqing, China). Thrombin binding aptamer (NH<sub>2</sub>-TBA): 5'-NH<sub>2</sub>-(CH<sub>2</sub>)<sub>6</sub>-GGTTGG TGT GGT TGG-3' was purchased from Sangon Biotech (Shanghai, China). Trishydroxymethylaminomethane hydrochloride (Tris-HCl) was from Roche (Switzerland). 20 mM Tris-HCl buffer (pH 7.4) containing 1 mM MgCl<sub>2</sub>, 1 mM CaCl<sub>2</sub>, 5 mM KCl and 140 mM NaCl was used as aptamer buffer. Phosphate buffered solution (PBS, pH 7.0), which contains 0.1 M Na<sub>2</sub>HPO<sub>4</sub>, 0.1 M KH<sub>2</sub>PO<sub>4</sub> and 0.1 M KCl, was employed as working buffer. All other reagents were of analytical-reagent grade and used as received. Double distilled water was used throughout the experiment.

### **Apparatus**

Differential pulse voltammetry (DPV) and cyclic voltammetry (CV) were conducted using a CHI 660D electrochemical workstation (Shanghai Chenhua Instrument, China) in a three electrode system. The working electrode used was a bare or modified glassy carbon electrode (GCE, 4 mm diameter). A platinum wire and a saturated calomel electrode (SCE) served as the auxiliary and the reference electrodes, respectively. Electrochemical impedance spectroscopy (EIS) was conducted using a CHI 660E electrochemical workstation (Shanghai Chenhua Instrument, China). The scanning electron micrographs were taken using scanning electron microscope (SEM, S-4800, Hitachi Instrument, Japan). The DPV measurements from -0.1 V to 0.6 V (vs. SCE) with the potential incremental of 4 mV, pulse width of 50 s, amplitude of 50

mV, and sample width of 0.0167 s, were performed in 1 mL PBS (0.1 M, pH 7.0) containing 3.68 mM H<sub>2</sub>O<sub>2</sub>. The CV scanning from -0.2 to 0.6 V at 100 mV/s scan rate and EIS measurements were carried out in 0.1 M PBS (pH 7.4) containing 5 mM K<sub>3</sub>[Fe(CN)<sub>6</sub>]/K<sub>4</sub>[Fe(CN)<sub>6</sub>]. X-ray photoelectron spectroscopy (XPS) measurements were carried out using the VG Scientific ESCALAB 250 spectrometer with Al K $\alpha$  X-ray (1486.6 eV) as the light source. pH measurement was conducted with a pH meter (MP 230, Mettler-Toledo, Switzerland).

### **Preparation of MWCNTs-MnO<sub>2</sub> nanocomposite**

Firstly, 0.5 g of multi-walled carbon nanotubes (MWCNTs) were treated with sonication in a mixture of H<sub>2</sub>SO<sub>4</sub> and HNO<sub>3</sub> (50 mL) in the ratio of 1:3 for 0.5 h. The mixture was heated to 90 °C and kept at this temperature for 1 h to obtain COOH-MWCNTs<sup>1</sup> for better dispersion. The product was cooled down to room temperature and washed with water repeatedly until the filtrate was neutral. Then, the obtained COOH-MWCNTs was dried under vacuum at 65 °C and subsequently dispersed in water to a concentration of 0.5 mg/mL for further use.

Secondly, APTES functionalized flower-like MnO<sub>2</sub> nanospheres (APTES-MnO<sub>2</sub>) was synthesized according to the previous literature with minor modification.<sup>2</sup> Briefly, 0.5 g of KMnO<sub>4</sub> was suspended in 250 mL of water with a magnetically stirring for 0.5 h. Oleic acid (5 mL) was added into the above solution and stirred for another 2.5 h to reduce KMnO<sub>4</sub>. When a steady emulsion was formed, the brown-black solid in the solution was collected by centrifuging at 12000 rpm for 10 min and washing with distilled water and alcohol to remove any possible residual reactants. The resulting

flower-like MnO<sub>2</sub> nanospheres was dried under vacuum at 60 °C. Then, APTES-MnO<sub>2</sub> was obtained by functionalizing MnO<sub>2</sub> nanospheres with APTES. A mixture of 0.25 g of the as-synthesized flower-like MnO<sub>2</sub> nanospheres, 0.5 mL of APTES and 80 mL of toluene was stirred and refluxed at 120 °C under N<sub>2</sub> for 6 h. After that, the obtained precipitate was centrifugated out, washed with toluene and water, resuspended in 12 mL of PBS (pH 7.4), and stored at 4 °C for further use.

Thirdly, 4 mg EDC and 1 mg NHS were added into 1 mL of the as-prepared COOH-MWCNTs. This was followed by addition of 300 µL of APTES-MnO<sub>2</sub> solution and stirring for 1 h at room temperature. The obtained MWCNTs-MnO<sub>2</sub> nanocomposite was stored at 4 °C for further use.

#### **Preparation of hemin/G-quadruplex conjugated MWCNTs-MnO<sub>2</sub>-PtNPs-Tb (secondary aptamer)**

Initially, 0.5 mL of H<sub>2</sub>PtCl<sub>6</sub> (w/w, 1%) was added dropwise into the as prepared MWCNTs-MnO<sub>2</sub> nanocomposite suspension and stirred for 10 min, followed by the slow addition of 1.25 mL of freshly prepared NaBH<sub>4</sub> (w/w, 1%). After reaction for 30 min, PtNPs were in situ generated by the redox reaction between PtCl<sub>4</sub><sup>2-</sup> and NaBH<sub>4</sub>. As a result, large amounts of PtNPs were immobilized onto the APTES-MnO<sub>2</sub> through the interaction between PtNPs and -NH<sub>2</sub> in APTES-MnO<sub>2</sub>. The resulting product was centrifuged and redispersed in 1 mL water. Subsequently, NH<sub>2</sub>-TBA (100 µL, 2.0 µM) and Tb (500 µL, 3 mM) were injected into the above MWCNT-MnO<sub>2</sub>-PtNPs solution and stirred overnight under 4 °C. Thus, Tb with -NH<sub>2</sub> group and NH<sub>2</sub>-TBA were attached onto MWCNTs-MnO<sub>2</sub>-PtNPs nanocomposite via the

interaction between PtNPs and  $-\text{NH}_2$  group. Then, 200  $\mu\text{L}$  of hemin (0.5 mg/mL) was added into the mixture with 40 min stirring at 4  $^\circ\text{C}$  to form the hemin/G-quadruplex structure. This was followed by the incubation of 50  $\mu\text{L}$  BSA (w/w, 1%) for 0.5 h to block the remaining active sites. The final product was centrifuged, resuspended in 1 mL water and stored in refrigerator (4  $^\circ\text{C}$ ) for further use.

For comparison experiment, the hemin/G-quadruplex conjugated MWCNTs-MnO<sub>2</sub>-Tb was synthesized according to the above mentioned method with a little modification: 300  $\mu\text{L}$  of APTES-MnO<sub>2</sub> solution was injected into 1 mL of the COOH-MWCNTs solution containing EDC (4 mg) and NHS (1 mg). After stirring for 1 h at room temperature, the sediment was collected by centrifugation and resuspended in 1 mL of water. Then, 100  $\mu\text{L}$  of NH<sub>2</sub>-TBA (2.0  $\mu\text{M}$ ), 500 of Tb (3 mM) and 100  $\mu\text{L}$  of GA (w/w, 1%) was added into the above solution and stirred overnight at 4  $^\circ\text{C}$ . Tb with  $-\text{NH}_2$  group and NH<sub>2</sub>-TBA were attached onto MWCNTs-MnO<sub>2</sub> nanocomposite with GA serving as a linking agent. Finally, 100  $\mu\text{L}$  of hemin (0.5 mg/mL) was added to the suspension with stirring under 4  $^\circ\text{C}$  for 2 h. The product was collected by centrifugation, redispersed in 1 mL of water and stored at 4  $^\circ\text{C}$  for further use. Besides, hemin/G-quadruplex conjugated MnO<sub>2</sub>-PtNPs-Tb, MWCNTs-MnO<sub>2</sub>- PtNPs-Tb-TBA, hemin/G-quadruplex conjugated PtNPs-Tb were also prepared by using the similar procedure.

### **Fabrication of the proposed electrochemical aptasensor**

A bear GCE was polished to a mirror-like surface with 0.3  $\mu\text{m}$  and 0.05  $\mu\text{m}$  Al<sub>2</sub>O<sub>3</sub> powder successively, followed by sonicating and rinsing thoroughly with double

distilled water. The GCE was dried in air at room temperature. In order to capture NH<sub>2</sub>-TBA, gold nanoparticles (AuNPs) were then electrodeposited on the GCE surface in HAuCl<sub>4</sub> solution at the potential of -0.2 V for 30 s. Next, the modified electrode was incubated with a 20 μL drop of NH<sub>2</sub>-TBA (2.5 μM) for 16 h at room temperature. It was then incubated with 20 μL of BSA solution (w/w, 1%) to block possible active sites against nonspecific adsorption. After incubating for 40 min, 20 μL of TB standard solutions with different concentrations were dropped onto the modified electrode for 40 min at room temperature. Ultimately, 20 μL of the secondary aptamer was placed onto the resulting modified electrode with incubation for 40 min. The physically absorbed species on the modified GCE were rinsed away with water after every assembly finishing.

## **RESULTS AND DISCUSSION**

### **Structure characterizations**

The procedure for the synthesis of MWCNTs-MnO<sub>2</sub>-PtNPs was monitored by using scanning electron microscope (SEM). As shown in Fig. S1A, the MnO<sub>2</sub> nanospheres with a size of about 100 nm exhibited a novel flower-like nanostructure which was formed by the self-assembly MnO<sub>2</sub> nanoplates.<sup>2</sup> Additionally, the SEM image of flower-like MnO<sub>2</sub> nanospheres showed distinct flower-like nanostructures of MnO<sub>2</sub> by comparison with that of APTES functionalized MnO<sub>2</sub> (Fig. S1B), revealing that APTES had been successfully captured onto the surface of the flower-like MnO<sub>2</sub> nanospheres during the modification process. From Fig. S1C, numerous flower-like

MnO<sub>2</sub> nanospheres were observed on the surface of MWCNTs, which indicated the formation of the MWCNTs-MnO<sub>2</sub> nanohybrid. Fig. S1D is the SEM image of MWCNTs-MnO<sub>2</sub>-PtNPs with the light color part being PtNPs, confirming the successful immobilization of PtNPs.

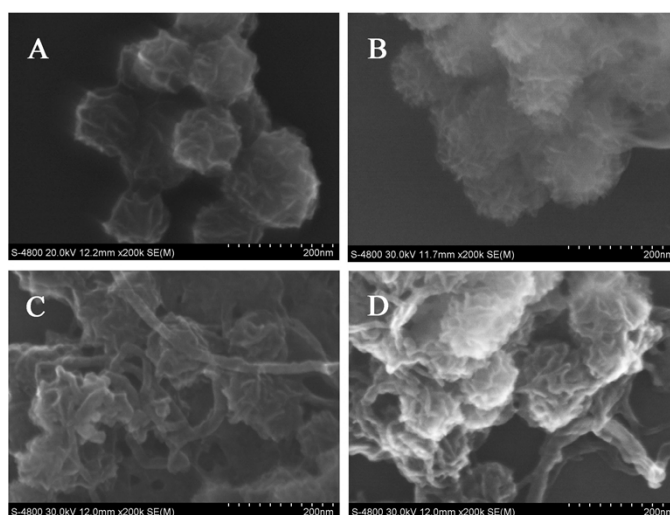


**Fig. S1** SEM images of (A) flower-like MnO<sub>2</sub> nanospheres, (B) APTES functionalized MnO<sub>2</sub>, (C) MWCNTs-MnO<sub>2</sub> and (D) MWCNTs-MnO<sub>2</sub>-PtNPs.

In addition, X-ray photoelectron spectroscopy (XPS) was employed to make further characterization of the as-prepared MWCNTs-MnO<sub>2</sub>-PtNPs-Tb nanocomposite. Fig. S2 showed the characteristic peaks of Mn2p (A) at 641.2 eV and 653.7 eV, O1s (B) at 531.2 eV, Si2p (C) at 101.9 eV, N1s (D) at 398.2 eV and C1s (E) at 284.3 eV, confirming the successful synthesis of MWCNTs-MnO<sub>2</sub> nanocomposite. Meanwhile, the characteristic peaks of Pt4f (F) were located at 71 and 74.2 eV, respectively, indicating the presence of PtNPs. Since the existence of S in redox-active Tb, the spectrum of S2p could be observed in Fig. S2(G), where the S2p spectrum appeared at 164 eV. All the above results indicate the successful preparation of MWCNTs-MnO<sub>2</sub>-

PtNPs-Tb nanocomposite.

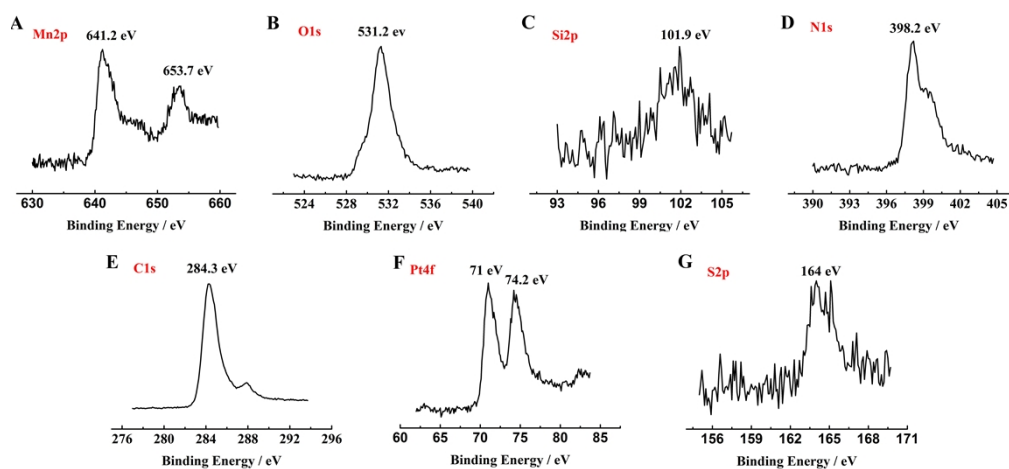


**Fig. S2** XPS spectra of (A) Mn, (B) O, (C) Si, (D) N, (E) C, (F) Pt, (G) S for MWCNTs-MnO<sub>2</sub>-PtNPs-Tb nanocomposite.

### EIS Characterization of the proposed aptasensor

To further gain insights on the changes of the electrochemical characteristics of the proposed aptasensor, electrochemical impedance spectroscopy (EIS) was recorded and shown in Fig. S3. The bare GCE exhibited a very small semicircle diameter (curve a). After electrodeposition of H<sub>2</sub>AuCl<sub>4</sub> (w/w, 1%), the semicircle diameter became smaller (curve b), indicating the good conductivity of AuNPs. The semicircle diameter apparently increased after the incubation of NH<sub>2</sub>-TBA onto the AuNPs layer (curve c), accounting for the presence of TBA which could block the electron transfer tunnel. When the inert BSA as blocking reagent was modified on the electrode, an increased semicircle diameter could be observed, owing to the increase of the resistance of the electrode surface. Besides, the semicircle diameter further increased after the introduction of TB (curve e) as a result of the successful immobilization of target TB which obstructed the electron transfer tunnel.

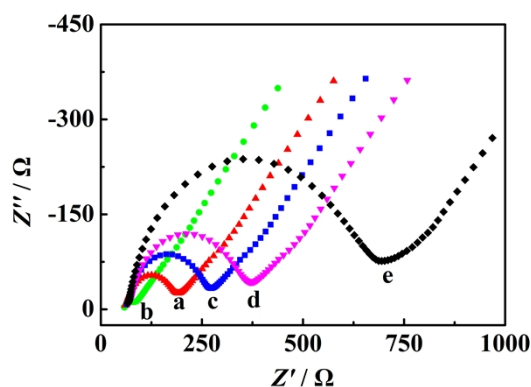


**Fig. S3** EIS characterization of different modified electrode in 5 mM  $K_3[Fe(CN)_6]/K_4[Fe(CN)_6]$ : (a) GCE, (b) AuNPs/GCE, (c)  $NH_2$ -TBA/AuNPs/GCE, (d) BSA/ $NH_2$ -TBA/AuNPs/GCE, (e) TB/BSA/ $NH_2$ -TBA/AuNPs/GCE. (220 mV potential with amplitude of 5 mV and frequency range of  $1.0 \times 10^{-2}$  Hz- $1.0 \times 10^6$  Hz, 2.5  $\mu$ M  $NH_2$ -TBA and 40 min TB incubation time.)

### Optimization of experimental conditions

The effect of  $NH_2$ -TBA concentration was firstly monitored via CV in 1 mL of 5 mM  $K_3[Fe(CN)_6]/K_4[Fe(CN)_6]$  solution. As shown in Fig. S4A, it can be seen that the current response decreased with the increase of  $NH_2$ -TBA concentration and the modification of the electrode reached saturation at 2.5  $\mu$ M. Thus, 2.5  $\mu$ M of  $NH_2$ -TBA was chosen as the optimal concentration for the construction of electrochemical aptasensor.

Another key factor for improving the sensitivity of the aptasensor is the incubation time of TB. From the results indicated in Fig. S4B, it was obvious that the peak current declined at the early stage of the reaction with the increase of the incubation time of TB up to 40 min, where a minimum peak current was obtained. Beyond a TB reaction time of 40 min, the CV response did not show further increase, indicating the

saturation binding of aptamer-TB. Hence, an incubation time of 40 min was employed as the optimum and applied for other investigations.

Additionally, the optimization of  $\text{H}_2\text{O}_2$  in testing buffer was also explored by conducting DPV experiments in 0.1 M PBS (pH 7.0) containing different concentrations of  $\text{H}_2\text{O}_2$  (from 2.22 mM to 4.14 mM). As could be seen in Fig. S4C, DPV response for TB decreased gradually with increasing  $\text{H}_2\text{O}_2$  concentration and reached a stable value at 3.68 mM, suggesting the highest electrocatalytic efficiency at this point. Therefore, 3.68 mM of  $\text{H}_2\text{O}_2$  was selected throughout the whole experiment.

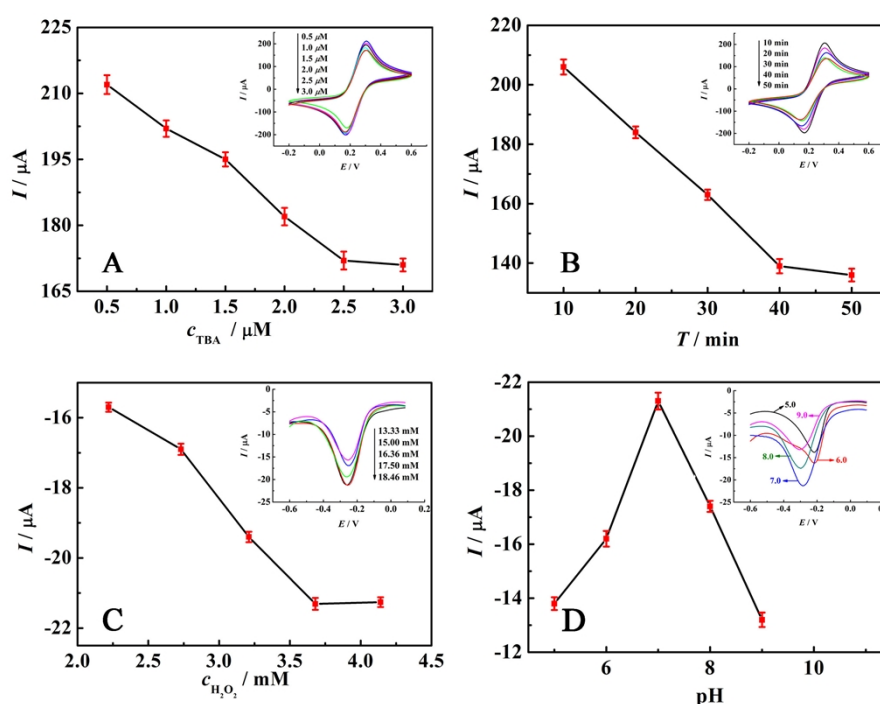


**Fig. S4** Effects of different experimental conditions on electrochemical response of the proposed aptasensor: (A)  $\text{NH}_2$ -TBA concentration and (B) incubation time of TB at 100 mV/s scan rate in 5.0 mM  $\text{K}_3[\text{Fe}(\text{CN})_6]/\text{K}_4[\text{Fe}(\text{CN})_6]$  (pH 7.4), (C)  $\text{H}_2\text{O}_2$  concentration in 0.1 M PBS (pH 7.0) and (D) pH of solution in 1.14 mL PBS (pH 7.0) containing 3.68 mM  $\text{H}_2\text{O}_2$ . Error bars: SD,  $n=3$ .

The pH of the detection solution was also optimized. Fig. S4D shows the influence of the pH of the testing buffer on the current responses of the fabricated aptasensor in the presence of 3.68 mM H<sub>2</sub>O<sub>2</sub> toward 10 nM TB. From Fig. S4D, it can be seen that the response current increased with increasing of pH value from 5.0 to 7.0 and then decreased. So, pH 7.0 of the working buffer was adopted for the subsequent investigation.

### **Comparison of TB aptasensors using different types of secondary aptamer bioconjugates**

For the successful development of a high sensitivity aptasensor, signal amplification is crucial. To verify the advantages of the as-synthesized hemin/G-quadruplex conjugated MWCNTs-MnO<sub>2</sub>-PtNPs-Tb, we also prepared another four types of secondary aptamer bioconjugates, i.e., MWCNTs-MnO<sub>2</sub>-PtNPs-Tb-TBA and hemin/G-quadruplex conjugated MWCNTs-MnO<sub>2</sub>-Tb, MnO<sub>2</sub>-PtNPs-Tb, PtNPs-Tb, respectively. Electrochemical detection for 10 nM TB was carried out in 1.14 mL PBS (0.1 M, pH 7.0) under optimal conditions and the results are showed in Fig. S5. As could be seen in Fig. S5, the aptasensor using hemin/G-quadruplex conjugated MWCNTs-MnO<sub>2</sub>-PtNPs exhibited higher reduction peak current and signal change than those of the other four aptasensing probes. The results suggested that the proposed secondary aptamer bioconjugates showed a significant electrocatalytic activity toward H<sub>2</sub>O<sub>2</sub> reduction, which may attribute to the following reasons: Firstly, the employment of MWCNTs with excellent conductivity can provide a large surface for the immobilization of biomolecules and enhance the electrocatalytic efficiency of

flower-like MnO<sub>2</sub> nanospheres and hemin/G-quadruplex. Secondly, the as-prepared flower-like MnO<sub>2</sub> nanospheres with large surface area not only act as a biomaterial to immobilize large amount of PtNPs, hemin/G-quadruplex and Tb, but also show remarkable catalytic activity toward H<sub>2</sub>O<sub>2</sub> reduction. Furthermore, the synergistic catalysis of PtNPs, hemin/G-quadruplex and flower-like MnO<sub>2</sub> nanospheres finally resulted in the greatly amplified detection signal and prominent sensitivity of the proposed aptasensor.

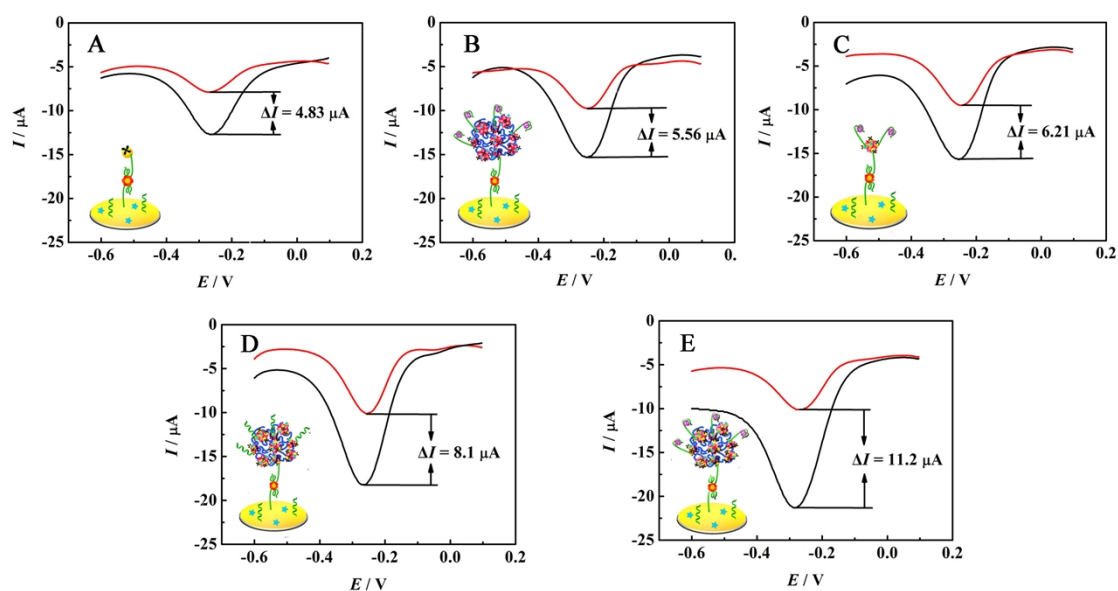


**Fig. S5** DPV responses of different strategies in the absence (red line) and in the presence (black line) of 3.68 mM H<sub>2</sub>O<sub>2</sub> in 1.14 mL PBS (0.1 M, pH 7.0) by using different secondary aptamers: (A) hemin/G-quadruplex conjugated PtNPs-Tb, (B) hemin/G-quadruplex conjugated MWCNTs-MnO<sub>2</sub>-Tb, (C) hemin/G-quadruplex conjugated MnO<sub>2</sub>-PtNPs-Tb (D) MWCNTs-MnO<sub>2</sub>-PtNPs-Tb-TBA and (E) hemin/G-quadruplex conjugated MWCNTs-MnO<sub>2</sub>-PtNPs-Tb. The concentration of NH<sub>2</sub>-TBA was 2.5 μM, and the incubation time of TB was 40 min.

**Table S1** Comparisons of the proposed aptasensor with different methodologies

Analytical methods	Linear range /nM	Detection limit /pM	Ref.
Fluorescence	0.6~100	0.2	3
EIS	0.12~30	0.30	4
Colorimetry	0.0025~6.2	1.5	5
CV	0.5~40	93	6
SV	10~10000	1000	7
DPV	1~60	0.5	8
DPV	0.0002~20	0.067	9
ECL	2~50	1300	10
DPV	0.0001~30	0.040	This work

**Abbreviation:** differential pulse voltammetry (DPV); cyclic voltammetry (CV); electrochemiluminescent (ECL); electrochemical impedance spectroscopy (EIS); stripping voltammetry (SV)

**Table S2** Performance of the proposed aptasensor compared with those of other

sandwich-type aptasensors for TB detection with DPV method

Materials	Enzymes	Linear range/nM	Detection limit/pM	Ref.
Hollow PtCo nanochains, bi-enzyme, hemin/G-quadruplex	Glucose oxidase	0.001~30	0.39	11
Iron telluride nanorods, hemin/G-quadruplex, thionine	Horseradish peroxidase	0.001~20	0.5	12
MWCNTs, amine-modified capture probe, ferrocene	— —	0.001~0.5	0.5	13
AuNPs, {nano-Au/thionine} <sub>n</sub> multilayer films, thionine	— —	0.12~46	40	14
PtNPs, graphene oxide, NiHCFNPs	Horseradish peroxidase	0.001~50	0.5	15
Flower-like MnO <sub>2</sub> nanospheres, PtNPs, hemin/G-quadruplex, toluidine blue	— —	0.0001~30	0.040	This work

**Table S3** Determination of TB in human blood serum ( $n=3$ ) with the proposed

electrochemical aptasensor<sup>a</sup>

Samples	Added TB/nM	Found TB/nM <sup>b</sup>	Recovery/%	RSD/%
1	0.001	0.00108	108	5.4
2	0.01	0.00990	99.0	7.1
3	0.1	0.109	109	4.6
4	1.0	0.106	106	6.3
5	10	9.75	97.5	6.7

<sup>a</sup>The experimental measurements were carried out by DPV in 0.1 M PBS (pH 7.0) containing 3.68 mM H<sub>2</sub>O<sub>2</sub>. <sup>b</sup>Calculated as a mean of three measurements.

## References

- 1 Y. S. Hwang, X. L. Qu and Q. L. Li, *Carbon*, 2013, **55**, 81–89.
- 2 Y. Zhang, M. Su, L. Ge, S. G. Ge, G. H. Yu and X. R. Song, *Carbon*, 2013, **57**, 22–33.
- 3 Q. L. Yue, T. F. Shen, L. Wang, S. L. Xu, H. B. Li, Q. W. Xue, Y. F. Zhang, X. H. Gu, S. Q. Zhang and J. F. Liu, *Biosens. Bioelectron.*, 2014, **56**, 231–236.
- 4 L. D. Li, H. T. Zhao, Z. B. Chen, X. J. Mu and L. Guo, *Sens. Actuators, B*, 2011, **157**, 189–194.
- 5 Y. Huang, J. Chen, S. L. Zhao, M. Shi, Z. F. Chen and H. Liang, *Anal. Chem.*, 2013, **85**, 4423–4430.
- 6 Z. Zhang, L. Q. Luo, L. M. Zhu, Y. P. Ding, D. M. Deng and Z. X. Wang, *Analyst*, 2013, **138**, 5365–5370.

- 7 E. Suprun, V. Shumyantseva, T. Bulko, S. Rachmetova and S. Rad'ko, *Biosens. Bioelectron.*, 2008, **24**, 825–830.
- 8 Y. N. Zheng, Y. Q. Chai, Y. L. Yuan and R. Yuan, *Anal. Chim. Acta*, 2014, **834**, 45–50.
- 9 Y. Kang, K. J. Feng, J. W. Chen, J. H. Jiang, G. L. Shen and R. Q. Yu, *Bioelectrochemistry*, 2008, **73**, 76–81.
- 10 G. X. Jin, L. J. Lu, X. Y. Gao, M. J. Li, B. Qiu, Z. Y. Lin, H. H. Yang and G. N. Chen, *Electrochim. Acta*, 2013, **89**, 13–17.
- 11 L. J. Bai, R. Yuan, Y. Q. Chai, Y. L. Yuan, Y. Zhuo and L. Mao, *Biosens. Bioelectron.*, 2011, **26**, 4331–4336.
- 12 L. P. Jiang, R. Yuan, Y. Q. Chai, Y. L. Yuan, L. J. Bai and Y. Wang, *Analyst*, 2013, **138**, 1497–1503.
- 13 X. R. Liu, Y. Li, J. B. Zheng, J. C. Zhang and Q. L. Sheng, *Talanta*, 2010, **81**, 1619–1624.
- 14 Y. L. Yuan, R. Yuan, Y. Q. Chai, Y. Zhuo, Z. Y. Liu, L. Mao, S. Guan and X. Q. Qian, *Anal. Chim. Acta*, 2010, **668**, 171–176.
- 15 Z. H. Xu, C. He, T. Sun and L. Wang, *Electroanalysis*, 2013, **25**, 2339–2344.